European Journal of Cardio-Thoracic Surgery 55 (2019) 1061–1070
doi:10.1093/ejcts/ezy399 Advance Access publication 6 December 2018

ORIGINAL ARTICLE

Cite this article as: van Bakel TMJ, Arthurs CJ, Nauta FJH, Eagle KA, van Herwaarden JA, Moll FL *et al.* Cardiac remodelling following thoracic endovascular aortic repair for descending aortic aneurysms. Eur J Cardiothorac Surg 2019;55:1061–70.

Cardiac remodelling following thoracic endovascular aortic repair for descending aortic aneurysms

Theodorus M.J. van Bakel[a,b,c,*], Christopher J. Arthurs[d], Foeke J.H. Nauta[a,b,c], Kim A. Eagle[e], Joost A. van Herwaarden[b], Frans L. Moll[b], Santi Trimarchi[c,f], Himanshu J. Patel[g] and C. Alberto Figueroa[a,h]

[a] Department of Surgery, University of Michigan, Ann Arbor, MI, USA
[b] Department of Vascular Surgery, University Medical Center Utrecht, Utrecht, Netherlands
[c] Thoracic Aortic Research Center, Policlinico San Donato IRCCS, San Donato Milanese, Italy
[d] Division of Imaging Sciences and Biomedical Engineering, King's College London, London, UK
[e] Department of Cardiology, University of Michigan, Ann Arbor, MI, USA
[f] Department of Biomedical Sciences for Health, University of Milan, Milan, Italy
[g] Department of Cardiac Surgery, University of Michigan, Ann Arbor, MI, USA
[h] Department of Biomedical Engineering, University of Michigan, Ann Arbor, MI, USA

* Corresponding author. Department of Surgery, University of Michigan, 2800 Plymouth Road B20-211W, Ann Arbor, MI 48105, USA. Tel: +1-734-5481660; fax: +1-734-2321234; e-mail: vanbakel@med.umich.edu (T.M.J. van Bakel).

Received 24 August 2018; received in revised form 27 October 2018; accepted 29 October 2018

Downloaded from https://academic.oup.com/ejcts/article/55/6/1061/5232605 by guest on 21 September 2020

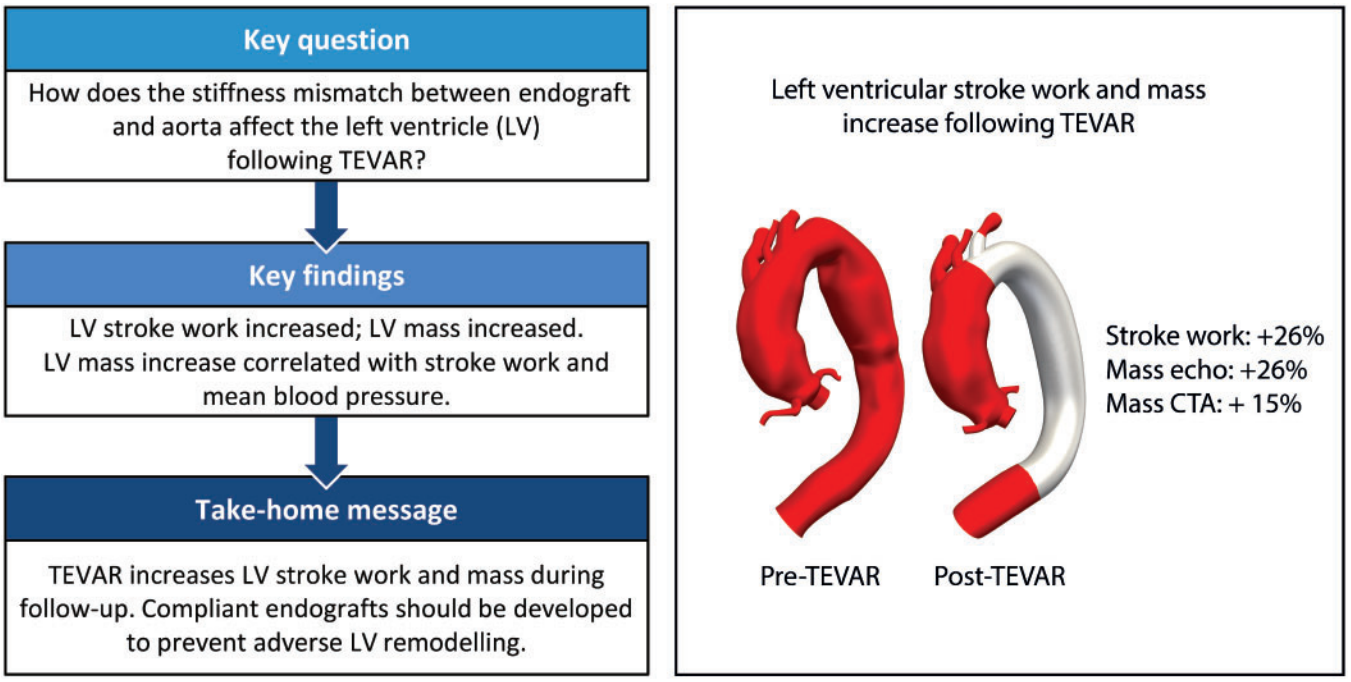

Abstract

OBJECTIVES: Current endografts for thoracic endovascular aortic repair (TEVAR) are much stiffer than the aorta and have been shown to induce acute stiffening. In this study, we aimed to estimate the impact of TEVAR on left ventricular (LV) stroke work (SW) and mass using a non-invasive image-based workflow.

Presented at the American Heart Association Scientific Sessions, Anaheim, CA, USA, 12 November 2017.

© The Author(s) 2018. Published by Oxford University Press on behalf of the European Association for Cardio-Thoracic Surgery. All rights reserved.

METHODS: The University of Michigan database was searched for patients treated with TEVAR for descending aortic pathologies (2013–2016). Patients with available pre-TEVAR and post-TEVAR computed tomography angiography and echocardiography data were selected. LV SW was estimated via patient-specific fluid–structure interaction analyses. LV remodelling was quantified through morphological measurements using echocardiography and electrocardiographic-gated computed tomography angiography data.

RESULTS: Eight subjects were included in this study, the mean age of the patients was 68 (73, 25) years, and 6 patients were women. All patients were prescribed antihypertensive drugs following TEVAR. The fluid–structure interaction simulations computed a 26% increase in LV SW post-TEVAR [0.94 (0.89, 0.34) J to 1.18 (1.11, 0.65) J, $P = 0.012$]. Morphological measurements revealed an increase in the LV mass index post-TEVAR of +26% in echocardiography [72 (73, 17) g/m^2 to 91 (87, 26) g/m^2, $P = 0.017$] and +15% in computed tomography angiography [52 (46, 29) g/m^2 to 60 (57, 22) g/m^2, $P = 0.043$]. The post- to pre-TEVAR LV mass index ratio was positively correlated with the post- to pre-TEVAR ratios of SW and the mean blood pressure ($\rho = 0.690$, $P = 0.058$ and $\rho = 0.786$, $P = 0.021$, respectively).

CONCLUSIONS: TEVAR was associated with increased LV SW and mass during follow-up. Medical device manufacturers should develop more compliant devices to reduce the stiffness mismatch with the aorta. Additionally, intensive antihypertensive management is needed to control blood pressure post-TEVAR.

Keywords: Thoracic endovascular aortic repair • Stroke work • Cardiac remodelling • Computational modelling

INTRODUCTION

Thoracic endovascular aortic repair (TEVAR) is the treatment of choice for descending thoracic aortic aneurysms [1]. Because of its superior early and mid-term outcomes over open surgery, the use of TEVAR is rapidly increasing [2]. The treatment range for TEVAR is extending with endografts deployed more proximally into the aortic arch and in younger patients [3–5]. Current endografts are made of materials much stiffer than the native thoracic aorta [6, 7]. These materials enhance the durability and reduce the risk of type IV endoleaks, but they stiffen the aorta. The aortic compliance serves a critical function to reduce the impedance and workload of cardiac ejection [8]. The healthy aorta stiffens with age, and this process is accelerated by smoking, high cholesterol, hypertension and genetic predisposition. Aortic stiffening is known to play a significant role in cardiovascular disease development and progression [8, 9]. Several preclinical studies have reported on acute stiffening of the aorta following TEVAR, resulting in acute elevated pulse pressure, hypertension, reduced coronary perfusion and eventually heart failure [10, 11]. These findings have been confirmed by computational studies using simplified blood flow models [12]. More recently, a clinical study revealed left ventricular (LV) remodelling in a mixed population of thoracic and abdominal aneurysm patients treated with endovascular repair using ultrasonography data to assess changes in aortic pulse wave velocity and myocardial mass [13].

The present study aimed to elucidate the impact of TEVAR-induced acute aortic stiffening on LV stroke work (SW) and mass using patient-specific fluid–structure interaction (FSI) analyses and image-based measurements of cardiac remodelling from echocardiography and computed tomography angiography (CTA) data.

MATERIALS AND METHODS

The University of Michigan Adult Cardiac Surgery database was retrospectively quarried for patients treated with TEVAR for the descending aortic aneurysms between 2013 and 2016. The following inclusion criteria were used: available pre-TEVAR and post-TEVAR echocardiography and CTA data. The exclusion criteria were aortic dissection, prior surgical or endovascular aortic repair, prior open-heart surgery, atrial fibrillation and echocardiographic ejection fraction of <50%. Approval was obtained from the institutional review board (HUM00112350), and the need for informed consent was waived. Information on demographics, medical and surgical history and clinical outcomes was retrieved.

Patient-specific computational modelling of haemodynamics

FSI techniques were used to simulate aortic haemodynamics, including interactions between blood, aorta and endograft using validated computational tools [14]. Patient-specific simulations were performed pre-TEVAR and post-TEVAR. Each simulation required the following: (i) a 3-dimensional model of the aorta and its side branches; (ii) stiffness properties of the vessel walls and endografts and (iii) the boundary conditions describing inflow and outflow waveforms.

Computational models of thoracic aorta, coronary arteries and the supra-aortic arteries were created from CTA data using the cardiovascular modelling software CRIMSON [15]. The workflow for this procedure is illustrated in Fig. 1. Figure 2 presents the pre-TEVAR and post-TEVAR geometrical models.

Wall thickness and stiffness were assigned to the different vessels using literature data, values and references that are reported in the Supplementary Material, Table S3. Figure 3 shows stiffness maps of the pre-TEVAR and post-TEVAR aorta for patient 4. The aortic wall thickness and stiffness were specified along the centre lumen line in all models. Pre-TEVAR, the thickness and stiffness at the level of the descending aortic aneurysm were set to 4.0 mm and 2.56 MPa, respectively, rendering a structural stiffness (i.e. the product of thickness and stiffness) of 10.2 MPa·mm. Post-TEVAR, thickness and stiffness at the level of the endograft were set to 2.8 mm and 55.2 MPa, respectively, rendering a structural stiffness of 154.6 MPa·mm. This is more than 15 times stiffer than the region of the aneurysm in the pre-TEVAR models.

Boundary condition specification and parameterization

As invasive pressure measurements of the LV were not available, we developed a workflow to estimate the LV end-diastolic pressure–volume (PV) relationship using image-based computational modelling. A 2-step approach was adopted to assign inflow and outflow boundary conditions. First, a preliminary FSI simulation was performed using aortic inflow duplex-Doppler

Downloaded from https://academic.oup.com/ejcts/article/55/6/1061/5232605 by guest on 21 September 2020

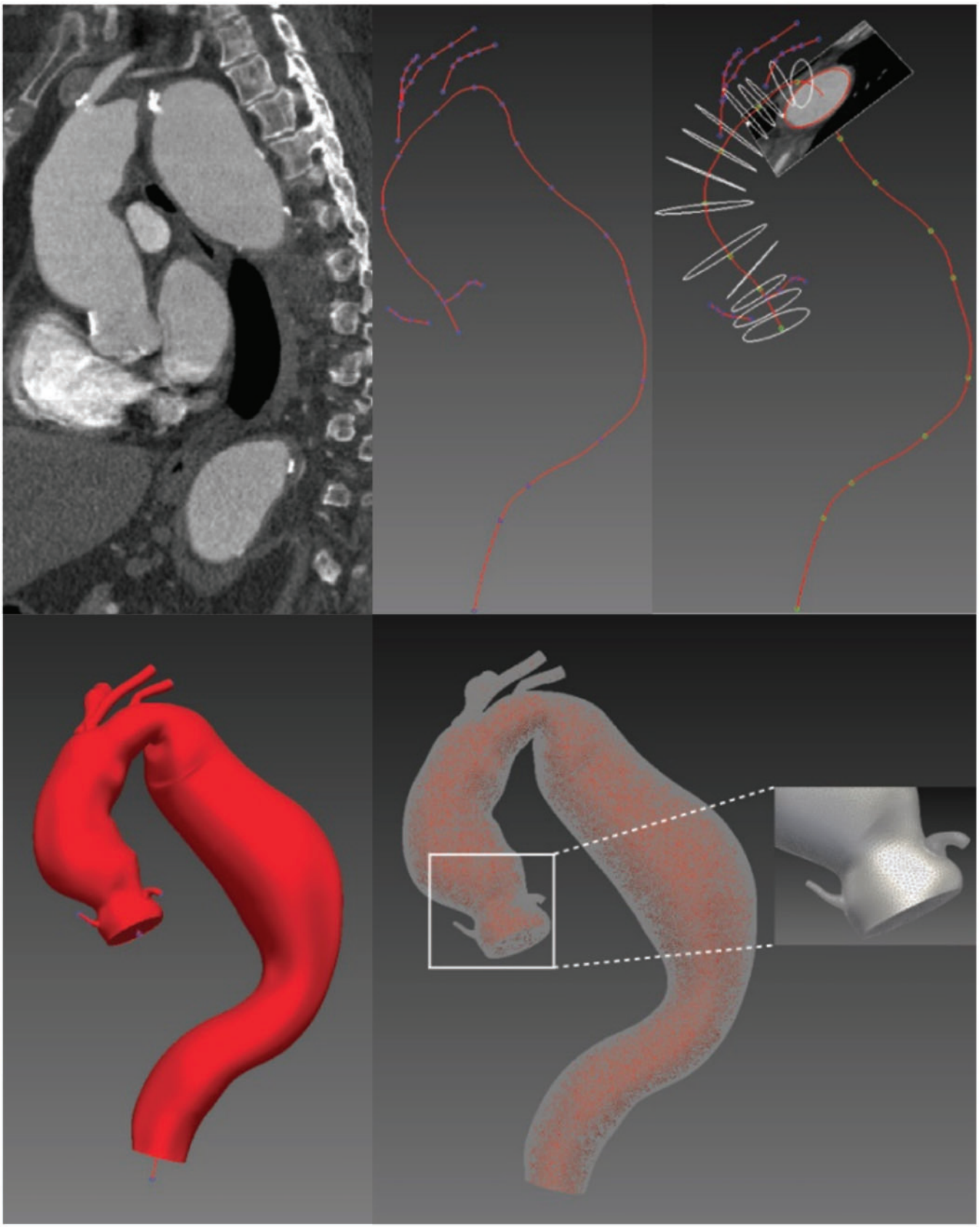

Figure 1: Patient-specific models of the thoracic aorta and its side branches were constructed from computed tomography angiography data. First, centre lumen lines were selected in each artery. Then, 2-dimensional segmentations were made along the centre lumen line, delineating the vessel walls. The individually segmented arteries were combined through an automated lofting and blending process, completing the 3-dimensional geometry. This geometry was then discretized into a highly refined finite-element mesh.

from https://academic.oup.com/ejcts/article/55/6/1061/5232605 by guest on 21 September 2020

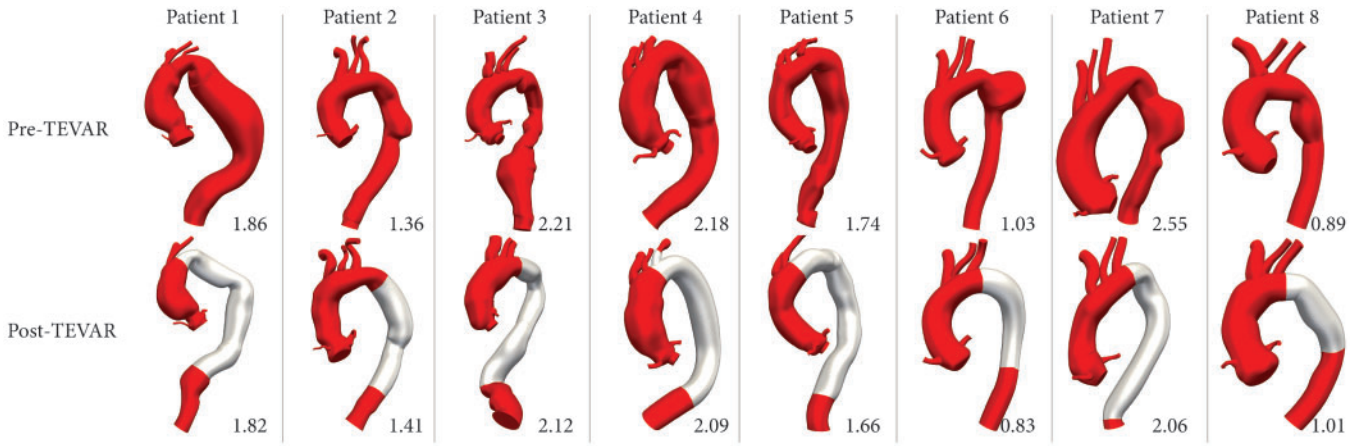

Figure 2: Pre-TEVAR and post-TEVAR geometric models for all patients. Finite-element mesh sizes are reported in millions of elements. TEVAR: thoracic endovascular aortic repair.

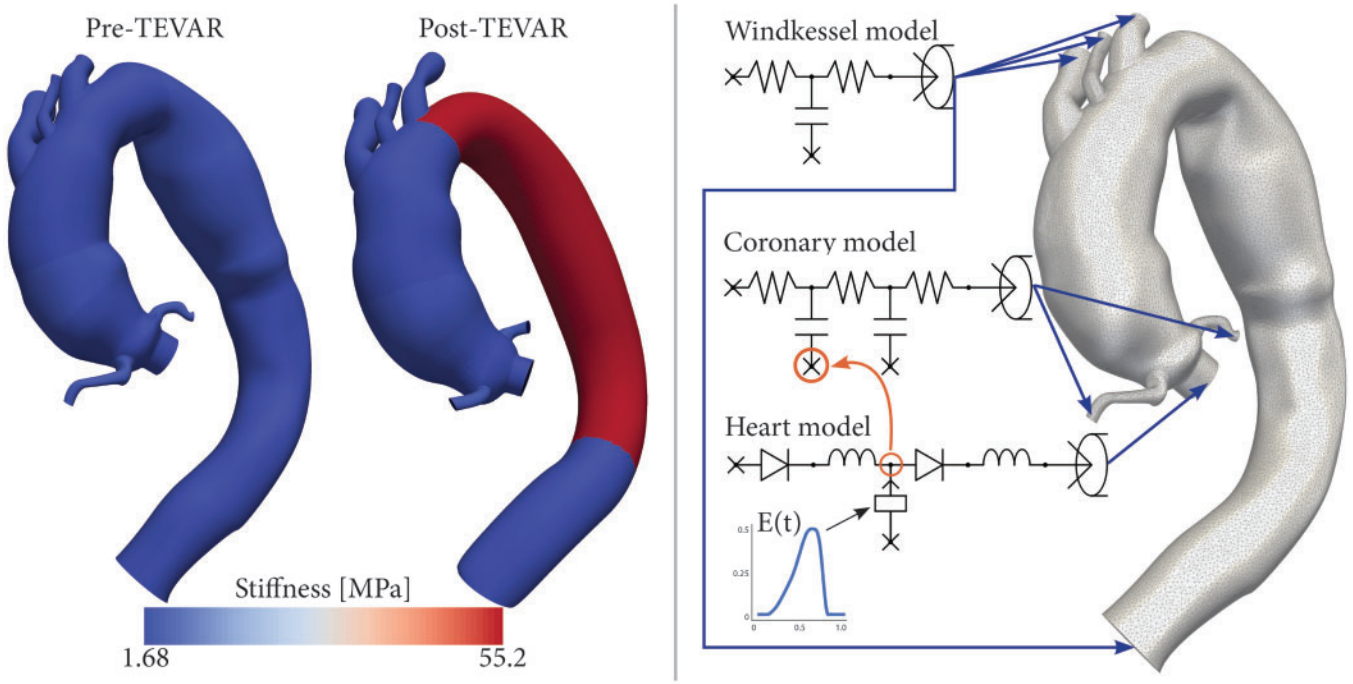

Figure 3: Left: distribution of the aortic and the endograft stiffness. Right: reduced order models were attached to the inflow and outflow sections of the 3-dimensional computational model. The parameters of the Windkessel, heart and coronary models were tuned to match the patient-specific flow and the pressure data. The patient-specific left-ventricular elastance function (E(*t*)) describes the pressure generation in the heart model. In the coronary circulation, extravascular myocardial compression is modelled by broadcasting the left ventricular pressure to each coronary model [16] (orange arrow). TEVAR: thoracic endovascular aortic repair.

echocardiography data to calculate the PV relationship in the aortic root. Then, these simulation results were used to calibrate a lumped-parameter heart model [16] that enabled quantification of LV SW. In the following, the methods of performing the preliminary simulation and constructing the heart model will be reviewed.

The pre-TEVAR and post-TEVAR cardiac outputs and inflow waveforms were derived from transthoracic duplex-Doppler echocardiography measurements at the LV outflow tract and imposed at the aortic root of the corresponding computational model. We did not have direct measurements of the flow and pressure waveforms at the side branches of the aorta. Therefore, we used the 3-element Windkessel models to represent the resistance and compliance of the distal vascular bed for each branch [17]. The parameters of the Windkessel models were iteratively tuned to match reported literature data on flow splits [18] and patient-specific brachial cuff blood pressure measurements that were taken at rest during the preoperative and follow-up office visit. Of note, the blood pressure measurements were routinely taken by the same staff, ensuring similar conditions between the consecutive measurements. The following flow splits were assigned as percentages of cardiac output: the brachiocephalic trunk 18%; the left common carotid artery 8%; the left subclavian artery 8%; the left coronary artery 4%; the right coronary artery 2% and the descending aorta 60%. If the left subclavian artery was over-stented during TEVAR, the left common carotid artery would be assigned 16% of the cardiac output.

Downloaded from https://academic.oup.com/ejcts/article/55/6/1061/5232605 by guest on 21 September 2020

Numerical values of pre-TEVAR and post-TEVAR Windkessel models for patient 4 are reported in the Supplementary Material, Tables S4 and S5.

The heart model

A lumped-parameter heart model including diodes and inductors to represent the mitral and the aortic valves, a pressure source representing the left atrial pressure and a volume-tracking pressure chamber representing the left ventricle was then calibrated and coupled to the inflow face of all aortic models (Fig. 3). The compliance and contractility of the pressure chamber are defined by a time-varying elastance function (E(*t*)) [16]. Patient-specific pre-TEVAR and post-TEVAR elastance functions were computed from the PV relationship at the aortic root in the preliminary simulations. When the aortic valve is open, the aortic root pressure provides an approximation of the LV pressure. The diastolic part of the elastance function was completed by assuming an exponential decay following the aortic valve closure to 5% of the peak elastance [19], followed by an exponential systolic rise until the aortic valve opening [19, 20]. Pre-TEVAR LV end-diastolic volume (EDV) was estimated for each patient using age, gender and body surface area (BSA) data [21]. As there is no significant change in BSA post-TEVAR, LV EDV was estimated from the echocardiography data using the modified Simpson's rule [22] as follows:

$$\text{Post}-\text{TEVAR EDV} = \text{Estimated Pre}-\text{TEVAR EDV}|_{\text{BSA}} \cdot \left(\frac{\text{Post}-\text{TEVAR EDV}}{\text{Pre}-\text{TEVAR EDV}}\right)|_{\text{Modified Simpon's rule}}$$

Estimated LV EDVs were compared with electrocardiographic (ECG)-gated CTA data whenever available. If the discrepancy between estimated and ECG-gated CTA ratios of post-TEVAR and pre-TEVAR EDV was larger than 5%, the ECG-gated CTA data were used. Numerical values of the lumped-parameter heart model for patient 4 are reported in the Supplementary Material, Table S6.

The coronary model

We used lumped-parameter models to represent the vascular beds of the left coronary artery and the right coronary artery (Fig. 3). The heart model enabled tracking of the LV pressure throughout the cardiac cycle. The LV pressure was broadcasted to a lumped parameter model of the left coronary artery to reproduce diastolically dominant coronary flow waveforms [16]. As the right ventricle operates at a lower pressure than the left ventricle, the LV pressure broadcasted to the right coronary artery coronary model was scaled down to 33%. These lumped-parameter models enable to capture the essential features of the coronary flow waveforms and, therefore, their impact on the ascending thoracic aortic haemodynamics.

Computations

Blood was modelled as an incompressible Newtonian fluid with a density of 1060 kg/m^3 and a dynamic viscosity of 4.0 mPa. Computations were performed using the CRIMSON flow solver on 80 cores at the University of Michigan High Performance Computing Cluster ConFlux. Typical computational time was 80 h per cardiac cycle. After the FSI simulations reached cycle-to-cycle periodicity and successfully reproduced patient-specific pressure and flow data within 5% margins, pre-TEVAR and post-TEVAR LV PV loops were generated from the heart models and the SW was calculated.

Cardiac remodelling

Changes in the LV mass were measured from pre-TEVAR and post-TEVAR echocardiography and ECG-gated CTA image data. Echocardiography examinations were performed by an independent operator. The LV mass (g) was calculated from the end-diastolic LV dimensions as follows [22]:

$$\text{LV mass} = 0.8 \cdot \left\{1.04[\text{LVID} + \text{PWT} + \text{SWT}]^3 - \text{LVID}^3\right\} + 0.6,$$

where LVID = LV internal diameter (mm), PWT = posterior wall thickness (mm) and SWT = septal wall thickness (mm).

In patients who had undergone ECG-gated CTA examinations, volumetric measurements of the LV myocardium were taken in the diastolic phase of the cardiac cycle, at 75% of the R-R interval using the automatic image processing tools in Vitrea (Vital Images Inc., Minnetonka, MN, USA) (Fig. 4). The LV mass was calculated from the product of the LV myocardial volume and the density of the myocardial tissue (1.04 g/cm^3) [23].

Statistical analysis

Analysis of the data was performed using the SPSS Statistics version 24 (IBM, Armonk, NY, USA). Continuous data are presented as mean (median, interquartile range). Comparisons between pre-TEVAR and post-TEVAR data were made using the Wilcoxon signed-rank test. Correlations were made using the Spearman's rank correlation coefficient. No correction was performed for multiple testing. All the statistical tests were 2-sided, and *P*-values $\leq$0.05 were considered statistically significant.

RESULTS

Study sample

In total, 195 patients were treated with TEVAR at the University of Michigan between 2013 and 2016. Eight patients met the inclusion and exclusion criteria, and 6 patients were women. The mean age of the patients was 68 (73, 25) years. The average time between the pre-TEVAR and the follow-up CTA scan was 458 (374, 562) days. A comparison of pre-TEVAR and post-TEVAR patient data is reported in Table 1. Additional information on patient selection and timing of the CTA and echocardiography examinations is reported in the Supplementary Material, Tables S1 and S2.

Computational outcomes

The pre-TEVAR and post-TEVAR simulation results successfully reproduced patient-specific data on pressure, stroke volume and EDV within 5% margins for all patients. Figure 5 demonstrates an example of pre-TEVAR and post-TEVAR waveforms in all the aortic branches for patient 4. LV SW increased in all patients post-TEVAR, and the mean SW increment was 26% [0.94 (0.89, 0.34) J to 1.18 (1.11, 0.65) J, *P* = 0.012]. Figure 6 presents a comparison of pre-

from https://academic.oup.com/ejcts/article/55/6/1061/5232605 by guest on 21 September 2020

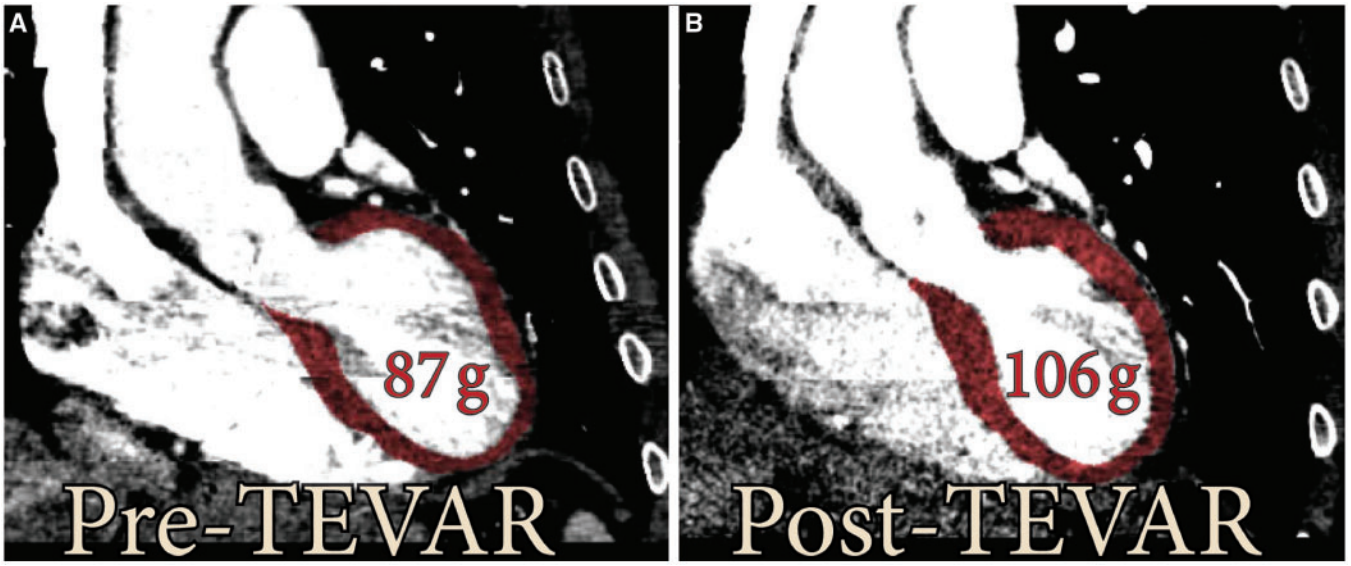

Figure 4: Left ventricular mass measurements from electrocardiographic-gated computed tomography angiography data pre-TEVAR (**A**) and post-TEVAR (**B**) in patient 4. TEVAR: thoracic endovascular aortic repair.

Table 1: Patient pre-TEVAR and post-TEVAR data

	Pre-TEVAR	Post-TEVAR	*P*-value
Physical examination (*n* = 8)			
Heart rate (beats/min)	71 (70, 12)	67 (68, 16)	
Systolic blood pressure (mmHg)	123 (123, 23)	146 (149, 29)	
Diastolic blood pressure (mmHg)	69 (71, 19)	79 (77, 15)	
Mean blood pressure (mmHg)	86 (85, 15)	100 (99, 22)	0.036
Pulse pressure (mmHg)	54 (52, 25)	67 (57, 36)	
BMI (kg/m^2)	28.2 (28.6, 12.1)	28.1 (26.1, 11.2)	
BSA (m^2)	1.93 (1.91, 0.44)	1.89 (1.90, 0.36)	
Echocardiography (*n* = 8)			
Cardiac output (l/min)	4.8 (4.5, 1.6)	4.9 (5.1, 2.2)	
Stroke volume (ml)	69 (62, 31)	73 (67, 25)	
LV end-diastolic volume (ml)	90 (91, 21)	100 (102, 14)	
LV fractional shortening (%)	43 (43, 17)	34 (34, 16)	
LV internal diameter systole (cm)	2.44 (2.37, 1.30)	2.90 (3.27, 1.10)	
LV internal diameter diastole (cm)	4.22 (4.23, 0.88)	4.43 (4.34, 1.37)	
Interventricular septum thickness (cm)	0.99 (0.93, 0.20)	1.18 (1.18, 0.47)	
LV mass index			
Echocardiography (g/m^2) (*n* = 8)	72 (73, 17)	91 (87, 26)	0.017
ECG-gated CTA (g/m^2) (*n* = 5)	52 (46, 29)	60 (57, 22)	0.043
Antihypertensive drugs (*n* = 8), *n* (%)			
B-blocker	4 (50.0)	7 (87.5)	
ACE-inhibitor	0 (0)	2 (25.0)	
Ca-channel blocker	3 (37.5)	2 (25.0)	
Angiotensin II receptor blocker	2 (25.0)	2 (25.0)	

Continuous data are presented as the mean (median, interquartile range).

ACE: angiotensin converting enzyme; BMI: body mass index; BSA: body surface area; CTA: computed tomography angiography; ECG: electrocardiography; LV: left ventricular; TEVAR: thoracic endovascular aortic repair.

TEVAR and post-TEVAR PV loops for all patients. There was no correlation between SW increment and endograft size.

Cardiac remodelling

Morphological measurements from echocardiography revealed a 26% increase in the LV mass index [72 (73, 17) g/m^2 to 91 (87, 26) g/m^2, $P = 0.017$] following TEVAR. There was a positive correlation between the ratio of post- to pre-TEVAR LV mass index and both the ratios of post- to pre-TEVAR LV stroke work and mean blood pressure ($\rho = 0.690$, $P = 0.058$ and $\rho = 0.786$, $P = 0.021$, respectively), Fig. 7. Volumetric measurements from ECG-gated CTA also revealed an increase in the LV mass index following TEVAR, albeit smaller than that obtained with echocardiography [+15%, 52 (46, 29) g/m^2 to 60 (57, 22) g/m^2, $P = 0.043$]. There was no correlation between post-TEVAR to pre-TEVAR LV mass index ratio and total endograft surface area for either echocardiography or CTA data.

Downloaded from https://academic.oup.com/ejcts/article/55/6/1061/5232605 by guest on 21 September 2020

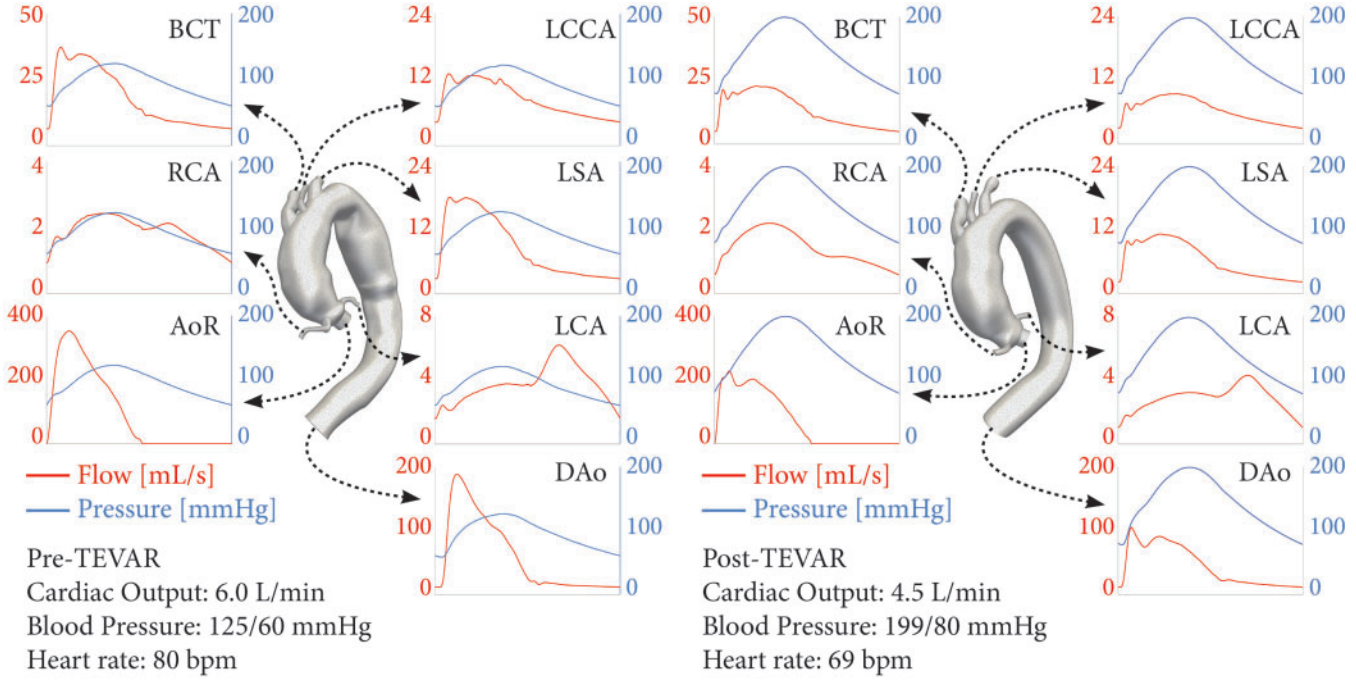

Figure 5: Flow and pressure waveforms for patient 4. AoR: aortic root; BCT: brachiocephalic trunk; DAo: descending aorta; LCA: left coronary artery; LCCA: left common carotid artery; LSA: left subclavian artery; LVOT: left ventricular outflow tract; TEVAR: thoracic endovascular aortic repair.

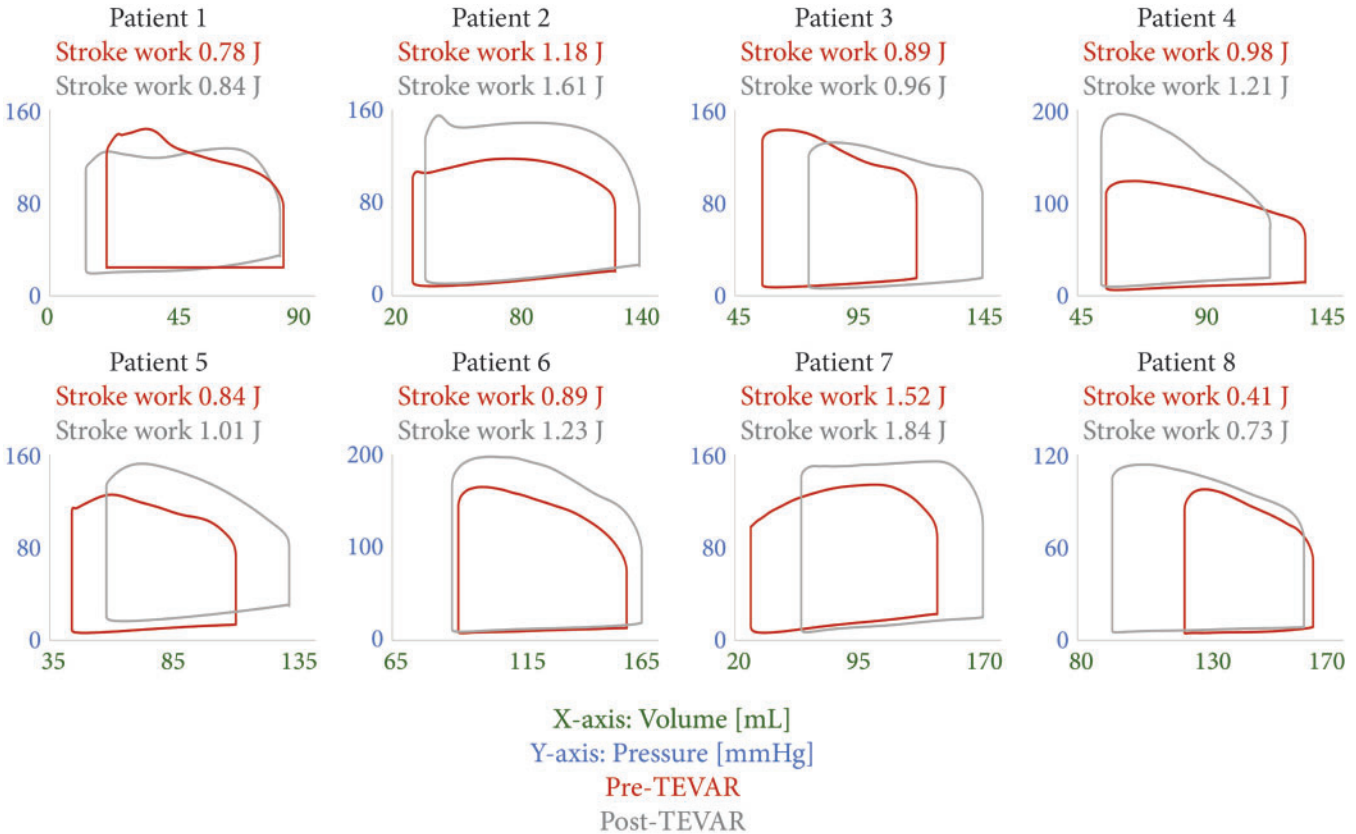

Figure 6: Comparison of pre- and post-TEVAR left ventricular pressure–volume loops. Stroke work is increased in all cases. Case-specific observations are discussed in the Supplementary Material. TEVAR: thoracic endovascular aortic repair.

from https://academic.oup.com/ejcts/article/55/6/1061/5232605 by guest on 21 September 2020

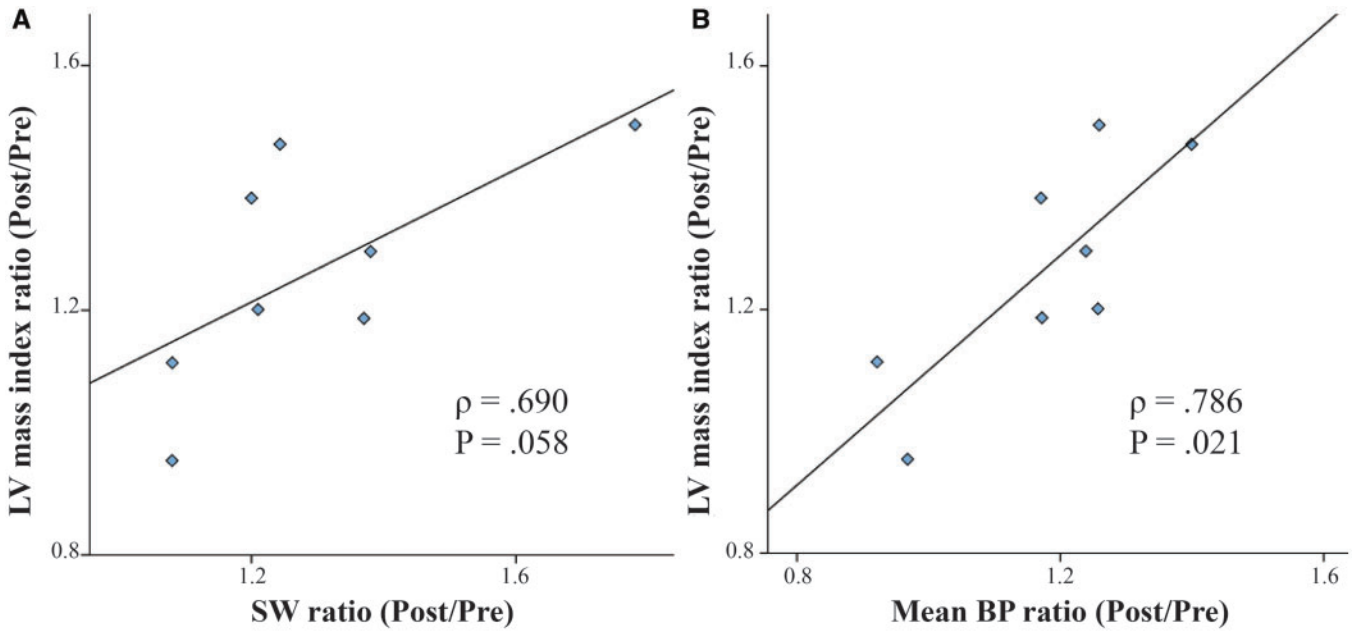

Figure 7: Positive correlation between the post- to pre-thoracic endovascular aortic repair mass index ratio measured by echocardiography and both SW and the mean BP ratio. BP: blood pressure; SW: stroke work.

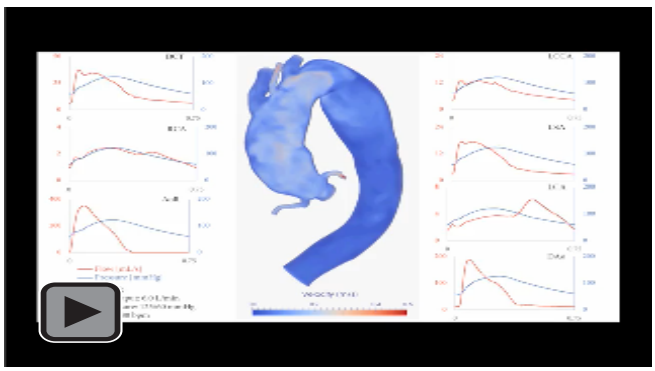

Video 1: Preoperative simulation results of one cardiac cycle in Patient 4. In the center, the three-dimensional anatomy is shown with a color-coded velocity mapping. Flow and pressure waveforms are reported at the in- and outlets of the model. AoR: aortic root; BCT: brachiocephalic trunk; DAo: descending aorta; LCA: left coronary artery; LCCA: left common carotid artery; LSA: left subclavian artery; RCA: right coronary artery; TEVAR: thoracic endovascular aortic repair.

DISCUSSION

The goal of the present study was to elucidate the effects of TEVAR-induced acute aortic stiffening on LV SW and remodelling. We present a workflow for non-invasive quantification of LV SW through patient-specific FSI analyses. Using this workflow, we unveiled a significant increase in LV SW post-TEVAR. The post-TEVAR to pre-TEVAR ratios of LV SW and LV mass index showed a positive correlation. Additionally, despite antihypertensive therapy, the mean blood pressure increased post-TEVAR. The post-TEVAR to pre-TEVAR ratios of the mean blood pressure and the LV mass index also showed a positive correlation.

The myocardial and aortic stiffening are well-known determinants of all-cause mortality and cardiovascular events [8, 24, 25]. Multiple clinical studies have reported increased pulse wave velocity and pulse pressure following endograft deployment [13, 26, 27]. In preclinical studies, similar effects were observed with additional findings of increased LV myocardial oxygen consumption and the LV mass [28, 29].

In this study, we confirmed the deleterious late consequences of increased *in vivo* impedance and stiffness mismatch after TEVAR on LV remodelling, using a computational modelling workflow that enabled us to quantify LV SW from non-invasive imaging and pressure data. Our findings suggest that medical device manufacturers should develop more compliant endografts for TEVAR to reduce the stiffness mismatch between the aorta and the device. Additionally, intensive antihypertensive therapy is needed to control blood pressure after TEVAR.

In some of our patients, we found that TEVAR resulted in a less tortuous configuration of the aortic lumen. We hypothesize that this could contribute to an overall reduction in LV SW despite the increase in aortic stiffness. This interplay between the aortic tortuosity and the stiffness will be a topic of future research, as it may have implications for patients presenting with pathologies compromising the lumen, such as the aortic dissection.

Limitations

As we did not have invasive measurements of the aortic pressure and the LV pressure available, we had to estimate the parameters for the heart model from echocardiography and CTA image data. This lack of data is most apparent in the end diastolic PV relationships depicted in Fig. 6, which were generated by similar assumptions regarding the exponential decay of the systolic part of the elastance function. Therefore, even though there is evidence of ventricular remodelling, the diastolic PV relationships do not reflect a stiffer behaviour. However, we admit that even with this imperfect definition of the diastolic part of the PV loops, our results reflect a clear trend in SW increase following TEVAR. Future studies are needed to calibrate this workflow using invasive pressure measurements in preclinical models or Doppler-derived atrioventricular pressure gradients.

Downloaded from https://academic.oup.com/ejcts/article/55/6/1061/5232605 by guest on 21 September 2020

The number of patients included in this study is relatively small, as the majority of patients who were treated at our institution were excluded (Supplementary Material, Fig. S1). We acknowledge this potentially induced selection bias. Furthermore, we performed a retrospective non-invasive analysis, and it was not possible to obtain the patient-specific tissue properties for our computational models. Therefore, we had to rely on literature data. Furthermore, we assigned the same flow splits to the outflow branches of all patients before and after TEVAR. By doing so, we assumed that TEVAR does not affect regional blood flow distributions. To overcome the aforementioned limitations, our group is currently recruiting patients for a prospective study in which additional flow, myocardial perfusion and myocardial strain measurements are acquired using the magnetic resonance imaging techniques [30].

Finally, running the FSI analyses is computationally expensive. Typically, simulation time of 2 weeks in a supercomputer was needed for each patient-specific FSI analysis. This limits their clinical applicability for now, but optimizations of computational methods or access to a larger computer hardware will make it possible to perform these simulations in clinically feasible time frames in future.

CONCLUSION

TEVAR increased LV SW and induced LV growth during follow-up. Medical device manufacturers should consider the impact of the stiffness mismatch between the graft material and the native aorta when developing new endografts for TEVAR, particularly considering the emerging role of endovascular repair in more proximal aortic segments and younger patient populations. Additionally, intensive antihypertensive therapy should prevent the increase in the mean blood pressure post-TEVAR.

SUPPLEMENTARY MATERIAL

Supplementary material is available at *EJCTS* online.

Funding

This work was supported by the European Research Council under the European Union's Seventh Framework Programme (FP/2007–2013) [ERC Grant Agreement No. 307532]; by grants from the National Institutes of Health [R01 HL105297, U01 HL135842]; the Edward B. Diethrich Professorship; the Bob and Ann Aikens Aortic Grants Program and the Frankel Cardiovascular Center. Funding sources also include the Joe D. Morris Professorship; David Hamilton Fund and the Phil Jenkins Breakthrough Fund. Computing resources were provided by the National Science Foundation [grant 1531752] Acquisition of Conflux, A Novel Platform for Data-Driven Computational Physics (Tech. Monitor: Ed Walker).

Conflict of interest: Kim A. Eagle received grants from W.L. Gore and Medtronic Inc. during the course of this study. Himanshu J. Patel serves as the consultant and the co-patent holder with W.L. Gore and the consultant for Medtronic Inc. and Terumo Inc. Santi Trimarchi serves as the consultant and the speaker for W.L. Gore and Medtronic Inc. Joost A. van Herwaarden serves as the consultant and the speaker for Bolton Medical, Cook Medical and Terumo Aortic. All authors declare the freedom of investigation and no conflict of interest is related to the contents of this manuscript.

REFERENCES

[1] Hiratzka LF, Bakris GL, Beckman JA, Bersin RM, Carr VF, Casey DE *et al.* ACCF/AHA/AATS/ACR/ASA/SCA/SCAI/SIR/STS/SVM guidelines for the diagnosis and management of patients with Thoracic Aortic Disease: a report of the American College of Cardiology Foundation/American Heart Association Task Force on Practice Guidelines, American Association for Thoracic Surgery, American College of Radiology, American Stroke Association, Society of Cardiovascular Anesthesiologists, Society for Cardiovascular Angiography and Interventions, Society of Interventional Radiology, Society of Thoracic Surgeons, and Society for Vascular Medicine. Circulation 2010;121:e266–369.

[2] von Allmen RS, Anjum A, Powell JT. Incidence of descending aortic pathology and evaluation of the impact of thoracic endovascular aortic repair: a population-based study in England and Wales from 1999 to 2010. Eur J Vasc Endovasc Surg 2013;45:154–9.

[3] Geisbüsch P, Kotelis D, Hyhlik-Dürr A, Hakimi M, Attigah N, Böckler D. Endografting in the aortic arch—does the proximal landing zone influence outcome? Eur J Vasc Endovasc Surg 2010;39:693–9.

[4] van Bakel TM, Arthurs CJ, van Herwaarden JA, Moll FL, Eagle KA, Patel HJ *et al.* A computational analysis of different endograft designs for Zone 0 aortic arch repair. Eur J Cardio Thorac Surg 2018; doi:10.1093/ejcts/ezy068.

[5] van Bakel TM, de Beaufort HW, Trimarchi S, Marrocco-Trischitta MM, Bismuth J, Moll FL *et al.* Status of branched endovascular aortic arch repair. Ann Cardiothorac Surg 2018; doi:10.3978/16472.

[6] Kleinstreuer C, Li Z, Basciano CA, Seelecke S, Farber MA. Computational mechanics of Nitinol stent grafts. J Biomech 2008;41:2370–8.

[7] Roccabianca S, Figueroa CA, Tellides G, Humphrey JD. Quantification of regional differences in aortic stiffness in the ageing human. J Mech Behav Biomed Mater 2014;29:618–34.

[8] Redheuil A, Wu CO, Kachenoura N, Ohyama Y, Yan RT, Bertoni AG *et al.* Proximal aortic distensibility is an independent predictor of all-cause mortality and incident CV events. The MESA Study. J Am Coll Cardiol 2014;64:2619–29.

[9] Humphrey JD, Harrison DG, Figueroa CA, Lacolley P, Laurent S. Central artery stiffness in hypertension and ageing a problem with cause and consequence. Circ Res 2016;118:379–81.

[10] Dobson G, Flewitt J, Tyberg JV, Moore R, Karamanoglu M. Endografting of the descending thoracic aorta increases ascending aortic input impedance and attenuates pressure transmission in dogs. Eur J Vasc Endovasc Surg 2006;32:129–35.

[11] Zacharoulis AA, Arapi SM, Lazaros GA, Karavidas AI, Zacharoulis AA. Changes in coronary flow reserve following stent implantation in the swine descending thoracic aorta. J Endovasc Ther 2007;14:544–50.

[12] Vardoulis O, Coppens E, Martin B, Reymond P, Tozzi P, Stergiopulos N. Impact of aortic grafts on arterial pressure: a computational fluid dynamics study. Eur J Vasc Endovasc Surg 2011;42:704–10.

[13] Takeda Y, Sakata Y, Ohtani T, Tamaki S, Omori Y, Tsukamoto Y *et al.* Endovascular aortic repair increases vascular stiffness and alters cardiac structure and function. Circ J 2014;78:322–8.

[14] Figueroa CA, Vignon-Clementel IE, Jansen KE, Hughes TJR, Taylor CA. A coupled momentum method for modeling blood flow in three-dimensional deformable arteries. Comput Methods Appl Mech Eng 2006;195:5685–706.

[15] CRIMSON. The Software for Cardiovascular Modelling and Simulation n.d. http://www.crimson.software (18 November 2018, date last accessed).

[16] Arthurs CJ, Lau KD, Asrress KN, Redwood SR, Figueroa CA. A mathematical model of coronary blood flow control: simulation of patient-specific three-dimensional hemodynamics during exercise. Am J Physiol Hear Circ Physiol 2016;310:H1242–58.

[17] Vignon-Clementel IE, Figueroa CA, Jansen KE, Taylor CA. Outflow boundary conditions for 3D simulations of non-periodic blood flow and pressure fields in deformable arteries. Comput Methods Biomech Biomed Engin 2010;13:625–40.

[18] Lantz BMT, Foerster JM, Link DP, Holcroft JW. Regional distribution of cardiac output: normal values in man determined by video dilution technique. Am J Roentgenol 1981;137:903–7.

from https://academic.oup.com/ejcts/article/55/6/1061/5232605 by guest on 21 September 2020

[19] Senzaki H, Chen C-H, Kass DA. Single-beat estimation of end-systolic pressure-volume relation in humans: a new method with the potential for noninvasive application. Circulation 1996;94:2497–506.
[20] Scalia GM, Greenberg NL, McCarthy PM, Thomas JD, Vandervoort PM. Noninvasive assessment of the ventricular relaxation time constant (tau) in humans by Doppler echocardiography. Circulation 1997;95:151–5.
[21] Maceira AM, Prasad SK, Khan M, Pennell DJ. Normalized left ventricular systolic and diastolic function by steady state free precession cardiovascular magnetic resonance. J Cardiovasc Magn Reson 2006;8:417–26.
[22] Lang RM, Bierig M, Devereux RB, Flachskampf FA, Foster E, Pellikka PA *et al*. Recommendations for chamber quantification: a report from the American Society of Echocardiography's guidelines and standards committee and the Chamber Quantification Writing Group, developed in conjunction with the European Association of Echocardiography. J Am Soc Echocardiogr 2005;18:1440–63.
[23] van Deel E, Ridwan Y, van Vliet JN, Belenkov S, Essers J. In vivo quantitative assessment of myocardial structure, function, perfusion and viability using cardiac micro-computed tomography. J Vis Exp 2016; doi: 10.3791/53603.
[24] Kingwell BA, Waddell TK, Medley TL, Cameron JD, Dart AM. Large artery stiffness predicts ischemic threshold in patients with coronary artery disease. J Am Coll Cardiol 2002;40:773–9.
[25] Watanabe H, Ohtsuka S, Kakihana M, Sugishita Y. Coronary circulation in dogs with an experimental decrease in aortic compliance. J Am Coll Cardiol 1993;21:1497–506.
[26] de Beaufort HWL, Coda M, Conti M, van Bakel TMJ, Nauta FJH, Lanzarone E *et al*. Changes in aortic pulse wave velocity of four thoracic aortic stent grafts in an *ex vivo* porcine model. PLoS One 2017;12: e0186080.
[27] Tzilalis VD, Kamvysis D, Panagou P, Kaskarelis I, Lazarides MK, Perdikides T *et al*. Increased pulse wave velocity and arterial hypertension in young patients with thoracic aortic endografts. Ann Vasc Surg 2012;26:462–7.
[28] Morita S, Asou T, Kuboyama I, Harasawa Y, Sunagawa K, Yasui H. Inelastic vascular prosthesis for proximal aorta increases pulsatile arterial load and causes left ventricular hypertrophy in dogs. J Thorac Cardiovasc Surg 2002;124:768–74.
[29] Kelly RP, Tunin R, Kass DA. Effect of reduced aortic compliance on cardiac efficiency and contractile function of in situ canine left ventricle. Circ Res 1992;71:490–502.
[30] Nauta FJH, Kamman AV, Ibrahim E-SH, Agarwal PP, Yang B, Kim K *et al*. Assessment of CardiOvascular Remodelling following Endovascular aortic repair through imaging and computation: the CORE prospective observational cohort study protocol. BMJ Open 2016; doi: 10.1136/bmjopen-2016-012270.

Downloaded from https://academic.oup.com/ejcts/article/55/6/1061/5232605 by guest on 21 September 2020